Article

Effect of pH Value on the Bandgap Energy and Particles Size for Biosynthesis of ZnO Nanoparticles: Efficiency for Photocatalytic Adsorption of Methyl Orange

Bachir Gherbi [1,2,3], Salah Eddine Laouini [1,2], Souhaila Meneceur [1,2], Abderrhmane Bouafia [1,2,*], Hadia Hemmami [1,2], Mohammed Laid Tedjani [1,2], Gobika Thiripuranathar [4], Ahmed Barhoum [5,6] and Farid Menaa [7,*]

1 Department of Process Engineering, Faculty of Technology, University of El Oued, El-Oued 39000, Algeria
2 Laboratory of Biotechnology Biomaterial and Condensed Matter, Faculty of Technology, University of El Oued, El-Oued 39000, Algeria
3 Unit of Renewable Energy Development in Arid Zones (UDERZA), University of El Oued, El-Oued 39000, Algeria
4 Institute of Chemistry Ceylon, College of Chemical Sciences, Welikada, Rajagiriya 10107, Sri Lanka
5 NanoStruc Research Group, Chemistry Department, Faculty of Science, Helwan University, Helwan 11795, Egypt
6 School of Chemical Sciences, Dublin City University, D09 V209 Dublin, Ireland
7 Department of Nanomedicine and Advanced Technologies, CIC-Fluorotronics, Inc., San Diego, CA 92037, USA
* Correspondence: abdelrahmanebouafia@gmail.com (A.B.); menaateam@gmail.com (F.M.)

Abstract: In this paper, ZnO nanoparticles (NPs) were greenly synthesized at different pH values of 4, 6, 9.5, and 11 via *Portulaca oleracea* leaf extract, and the effect of pH on the optical and structural properties was studied. UV-Vis spectrophotometers and FTIR spectroscopy characterized the optical properties. Meanwhile, the structural properties were characterized via Scanning Electron Microscopy (SEM) and X-ray Diffraction (XRD). Furthermore, their photocatalytic dye degradation was examined against methyl orange dye. The characterization results have confirmed the successful biosynthesis of ZnO nanoparticles with a size ranging between 22.17 to 27.38 nm. The synthesis pH value significantly influenced ZnO NPs' optical and morphological properties. The results have also indicated the high performance of the greenly synthesized ZnO NPs for dye degradation.

Keywords: green synthesis; *Portulaca oleracea*; zinc oxide; metallic nanoparticles; photocatalysis; methyl orange; sustainability

1. Introduction

Nanomaterials and nanotechnologies are raising significant hopes because of the specific properties of matter at the nanometric scale, which make it possible to envisage new functions that were unimaginable until now [1]. ZnO nanoparticles (NPs) are notable among them, with great interest due to their unique properties. ZnO is a non-toxic multifunctional inorganic material with a wide range of uses in several fields [2]. ZnO is a wurtzite type light electronic and photonic semiconductor with a high exciton binding energy (60 meV) at room temperature and a large direct bandgap of 3.37 eV [3,4]. The strong binding energy of ZnO excitons allowed excitonic evolutions even at room temperature. This could notify a strong radiative recombination yield for natural emission and a low threshold voltage for laser emission. The absence of a center of symmetry in wurtzite, combined with a remarkable electromechanical coupling, results in strong piezoelectric and pyroelectric properties, which makes using ZnO favorable in mechanical actuators and piezoelectric sensors [5,6]. Previous studies have confirmed that green synthesized ZnO NPs have significant photocatalytic, anticancer, antioxidant, and antibacterial activities,

which has made them widely used in manufacturing several drugs and of great interest to researchers [7,8]. The plant *Portulaca oleracea* L. (purslane) grows sufficiently across various regions of the world, including Algeria. (known as Régla). The seeds and leaves of *Portulaca oleracea* L. have various therapeutic applications, including diuretic, antiasthmatic, antipyretic, anti-inflammatory, and antitussive uses [9]. In addition, several studies have confirmed various pharmacological consequences of *Portulaca oleracea* L. in conjunction with hypoglycemic agents [10], Type 2 diabetes mellitus care [11], hypocholesterolemic [12], and against influenza A viruses [13], and antioxidant [14]. The *Portulaca oleracea* L. has various bio-compounds such as omega-3 fatty acids (α-linolenic acid, linolenic acid), in addition to alkaloids, flavonoids, coumarins, phenolic compounds (p-hydroxybenzoic and protocatechuic acids [15], It has been mentioned that *purslane* seeds are more reliable than other parts [16]. Due to increased antibiotic resistance, using metal oxide NPs can be a competent option.

Previous studies have indicated that the morphology of the biosynthesized metal oxide nanoparticles significantly depends on the amount of H^+ or OH^- ions presented [17]. The prementioned ions are essential to determine the metal-oxygen bond polymerization over the zinc oxide growth process [18]. Therefore, hydrolysis and condensation reactions occurring in the precursor solution formation are strongly affected by the variation in the pH value of the solution [19]. This distinction in pH further influences biosynthesized nanoparticles' morphology and their properties, including optical properties [20].

This study presents an efficient and sustainable strategy for biosynthesizing ZnO NPs from Zinc Acetate dihydrate ($Zn(CH_3COO)_2 \cdot 2H_2O$) solution using *Portulaca oleracea* leaves extract. To the best of our knowledge, this is the first study that looked at the effects of pH values of 4, 6, 9.5, and 11 on ZnO NP production, optical properties, and catalytic activity toward the degradation of methyl orange. MO dye was chosen for this study as it is the most widely used azo dye in the textile industry. At the same time, it can cause genetic changes in cells. This chemical is poisonous and has yellowish qualities. The biodegradable and detoxifying effects of ZnO NPs on the breakdown of methyl orange dye are examined in this study at varied reaction times.

2. Experimental

2.1. Chemicals, Reagents, and Plant Materials

Portulaca oleracea leaves were collected from El Oued, Southeast Algeria. Zinc Acetate ($Zn(CH_3COO)_2 \cdot 2H_2O$, 98%) and sodium borohydride ($NaBH_4$ 99%) were purchased from Sigma-Aldrich, Germany. Distilled water was used in all the experiments. India supplied the MO dye.

2.2. Preparation of Plant Extract and Analysis

First, 250 g of fresh *Portulaca oleracea* leaves were washed with distilled water and left for 15 min without stirring at room temperature. They are then crushed, the extracts are then filtered, and an amount of distilled water is added until the mixture reaches 1000 mL.

Each time, the pH was measured and then adjusted the dose to obtain the required pH by adding sodium borohydride ($NaBH_4$) solution to achieve the required pH (pH = 4, 6, 9.5, and 11) and stored in a glass container at 4 °C for later use.

2.3. Green Synthesis of Zinc Oxide Nanoparticles

For the synthesis of ZnO NPs, modified protocols from previous studies were adopted [21–26]. The Zinc Acetate ($Zn(CH_3COO)_2 \cdot 2H_2O$) solution was prepared using distilled water. $NaBH_4$ solution was used to adjust the pH (4, 6, 9.5, and 11). After that, 3 g of $Zn(CH_3COO)_2 \cdot 2H_2O$ was added to the mixture of the extract in a volume ratio of 1:10 (*v/v*) between extract and $Zn(CH_3COO)_2 \cdot 2H_2O$, then stirred and heated at a temperature of 70 °C for 120 min. We collected the solid product using centrifugation for 15 min at 5000 rpm and washed it three times with sterile deionized water. The product was dried

overnight at 80 °C and then calcined in a furnace at 500 °C for 2 h. We stored the resulting powder in containers for different characterizations and then used it for characterization.

2.4. Characterization of Zinc Oxide Nanoparticles

X-Ray Diffraction (XRD, RigakuMiniflex 600) with a Cu-K (λ = 1. 15418 Å) was used to study the crystalline structure of ZnO NPs. A scanning electron microscope was used to examine the particle size and shape (SEM, TESCAN VEGA 3). In the spectral region of 4000–500 cm^{-1}, a Fourier transform infrared spectrometer (FTIR, Nicolet iS5, Thermo Fisher Scientific) was used to examine the bonding characteristics of ZnO/NPs. The UV-vis absorption spectrum (Shimadzu-1800) in the wavelength range of 200–900 nm was used to estimate the light absorbance and bandgap energy of ZnO NPs.

Using the Scherrer formula (Equation (1)), the crystallite size was estimated by picking the dominant peak with the greatest intensity

$$D = \frac{k\,\lambda}{\beta\,\cos\theta} \tag{1}$$

where D is the crystallite size, k denotes the so-called shape factor (0.9), λ is the wavelength (0.15418 nm, CuK), β is the Full Width at Half Maximum (FWHM), θ and is the diffraction angle.

2.5. Photocatalytic Degradation of Methyl Orange

Green synthesized ZnO NPs produced at various pH values (4, 6, 9.5, and 11) were used to assess Methyl Orange (MO) photodegradation [27]. All experiments were conducted under sunlight [28]. Initially, a solution was prepared by adding 5 mg of ZnO NPs to 10 mL of MO solution (2. 5×10^{-5} M). Then the mixture was stirred constantly for about 30 min in darkness during the reaction, placed under the sun, stirring at about 30 °C. The centrifugal MO solution was used to measure the degradation. The absorbance of the solution was measured at λmax = 464 nm and 272 nm [29] at various times (5, 10, 20, 30, 60, and 120 min) intervals were measured with the UV–visible spectrophotometer (SHIMADZU 1800). The amount of adsorption at equilibrium is calculated using Equation (2) qe (mg/g):

$$qe = \frac{(C_0 - Ce)V}{m} \tag{2}$$

C_0 and Ce (mg/L) represent the initial concentration and the equilibrium liquid phase dye concentration. While V represents the solution's volume (L), and m represents the mass of adsorbents (g).

The degradation efficiency was calculated using the equation below:

$$\% \text{ degradation} = \frac{(C_0 - C_t)}{C_0} \times 100 \tag{3}$$

where C_t is the residual concentration in solution at a given time (t), and C_0 is the starting concentration (t).

3. Results and Discussion

Green synthesis of metallic NPs (e.g., ZnO NPs) by lower (e.g., algae) or higher plants such as *Portulaca oleracea* is more efficient than chemical and physical synthesis, as scientists have agreed that green synthesis is a clean, non-toxic, cost-effective, and an eco-friendly approach [30]. Furthermore, *Portulaca oleracea* grows randomly in nature and is abundantly available, making it a preferred botanical source for large-scale green synthesis of metallic NPs [31,32]. Recent studies have proven that the biosynthesis of ZnO NPs depends on the secondary metabolites present in the extract, which are the main ones responsible for reducing metal ions [33]. The change in color of the solution from green to brown within 30 min is the most noticeable visual observation during the reaction. The brown color indicates that ZnO NPs are being synthesized. In our study, we proposed a possible

mechanism for reducing Zn^{2+} to $Zn(0)$ by secondary metabolites present in *Portulaca oleracea* leaf extract, thus forming ZnO NPs.

3.1. Crystal Structure and Composition

The diverse chemical composition of *Portulaca oleracea* is ascribed to its medicinal power; it is rich in primary and secondary metabolites, as well as minerals, vitamins, and other micronutrients.

Portulaca oleracea L. has a considerable amount of polyphenols and flavonoids (genistein, myricetin, portulacanones, quercetin, kaempferol, apigenin, genistin, luteolin A to D, and others), phenolic acids, lignins, and stilbenes, according to chemical analysis [14,34].

Figure 1 shows an XRD study of biosynthesized ZnO NPs at different pH values (4, 6, 9.5, and 11). A biosynthetic investigation of ZnO NPs by *Portulaca oleracea* leaf extract displays four strong, distinctive Bragg reflection peaks in all patterns.

As can be seen from XRD patterns shown in Figure 1, all the samples exhibited common peaks located at two θ positions of 31.8°, 34.46°, 36.29°, 47.59°, 56.65°, 62.93°, 66.45°, 68.02°, 69.14°, 72.68°, 77.05° which are attributed to the crystal planes 100, 002, 101, 012, 110, 013, 200, 112, 201, 004, 011, respectively, where ZnO NPs had a hexagonal crystal structure (Space group P 63 m c (186) and lattice parameters of a = 3.24940 Å c = 5.20380 Å) JCDPS [35]. The samples have different crystallite sizes ranging from 22.17 nm to 27.38 nm Table 1.

The larger the crystals are, as seen in Figure 1, the higher the peak intensity. This supports the hypothesis that the lower the potential hydrogen pH values (4, 6, 9.5, and 11), the larger the crystal size. Increasing the pH has already been shown to reduce crystallite size. The size of nanoparticles is affected by pH. At high pH reduction rate is high. Instead of reduction, oxidation will occur at low pH ≤ 5. At very high pH ≥ 9, 10, the reduction rate will be too fast, resulting in nanoparticle aggregation. As a result, pH = 8 is preferred for producing smaller nanoparticles. As pH controls not only the size of the nanoparticles, but it also plays a significant role in the prevention of extra site products, which are minimized at neutral pH of 7–8. Extra site products act as impurities in your desired product.
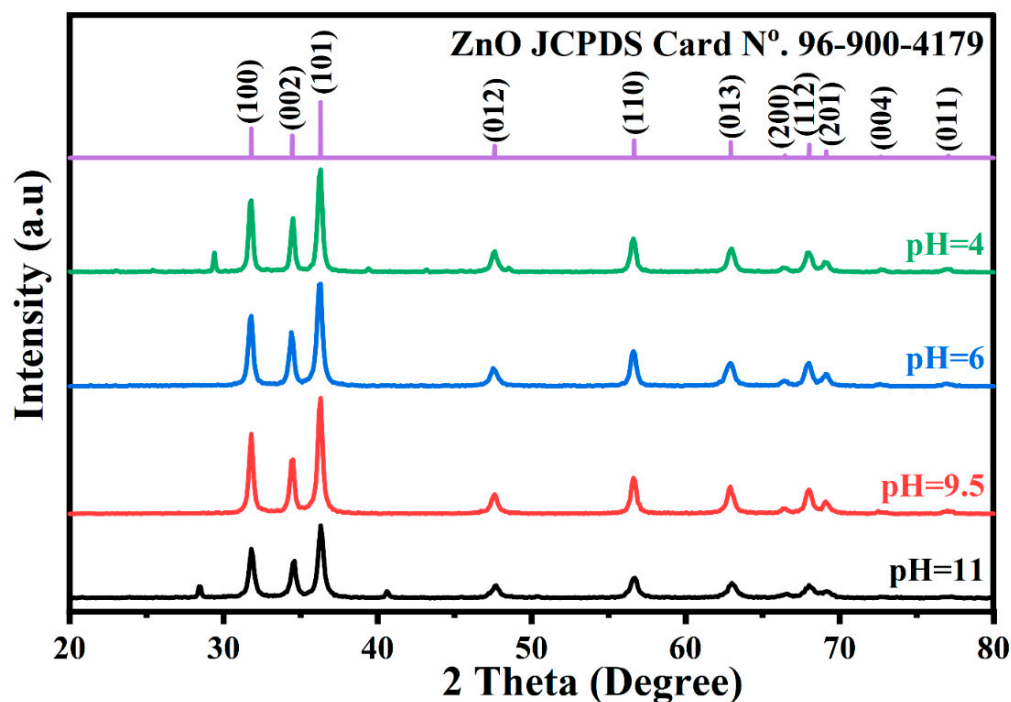

Figure 1. X-ray diffraction patterns of the zinc oxide nanoparticles with different pH values.

Table 1. Crystallite size of zinc oxide NPs obtained by different pH values.

Sample Name	FWHM	2 Theta	Crystallite Size (nm)	Phases	Reference	Lattice	Lattice Parameters	Space Group
pH = 11	0.4	36.33	22.17	ZnO + impurities	[35]	hexagonal	a = 3.24940 Å c = 5.20380 Å	P 63 m c (186)
pH = 9.5	0.344	36.27	25.39	ZnO	[35]	hexagonal	a = 3.24940 Å c = 5.20380 Å	P 63 m c (186)
pH = 6	0.38	36.23	26.04	ZnO	[35]	hexagonal	a = 3.24940 Å c = 5.20380 Å	P 63 m c (186)
pH = 4	0.319	36.26	27.38	ZnO + impurities	[35]	hexagonal	a = 3.24940 Å c = 5.20380 Å	P 63 m c (186)

3.2. FTIR Spectroscopy Analysis

FTIR spectrophotometric measurements of the leaf extract of *Portulaca oleracea L.* and the synthesized ZnO NPs were performed at various pH values to obtain more information about the phytochemical compounds responsible for the green synthesis of ZnO NPs.

In this work, the IR recorded distinct bands for the functional groups of the phytochemical compounds that are responsible for the biosynthesis of ZnO NPs as capping and stabilizing agents.

Bands and functional groups in *Portulaca oleracea* L. leaf extract were analyzed using FTIR. The FTIR analysis revealed that several functional groups, such as phenols, carboxylic acids, alkenes, aldehydes, and alkanes, were present in the aqueous leaves extract.

The characteristic FTIR showed a strong absorption band at 3293 cm^{-1} in *Portulaca oleracea L.* whose intensity has reduced until it completely disappears after the calcination process. The band at 3293 cm^{-1} may be attributed to the OH stretching and N–H [36] as shown in Figure 2. The band at 2331cm^{-1} are the characteristic peaks for the C≡C stretching. The band at 1605 cm^{-1} can be attributed to the aromatic amine's C-N stretching vibration and the (C=O) stretching vibration of the amide carbonyl [37]. The band at 630 cm^{-1} corresponds to the aromatic (C-H) group [38].

The leaf extract of *Portulaca oleracea L.* includes around 400 phenolic and flavonoid components, as well as other chemical constituents such as steroids, vitamins, minerals, fatty acids, alkaloids, saponins, and other chemicals. Flavonoids, in particular, have a fifteen-carbon structure that consists of two phenyl rings connected by three carbon atoms to form an oxygenated heterocycle [39].

Figure 2 shows the FTIR spectra of ZnO NPs biosynthesized at various pH values (4, 6, 9.5, and 11). The band centered at 474 cm^{-1} is attributed to the ZnO NPs stretching vibrations; the previous study has shown similar results [40,41].
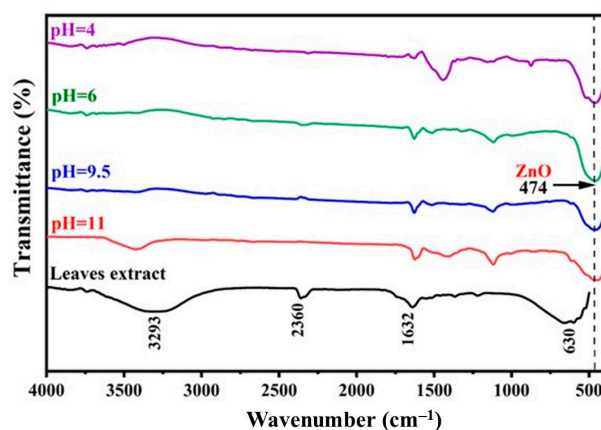

Figure 2. FTIR spectrum of ZnO NPs at different pH values, after annealing at 500 °C in air atmosphere and Portulaca oleracea L. leaf extract.

3.3. Morphological Investigation

The morphology and size of ZnO NPs are affected by several parameters in the green synthesis of NPs, the most important of which are the pH of the solution, the temperature of the reaction, the annealing, the stirring, the concentration of the extract, and the concentration of the salt, according to studies (source of mineral precursor salts). In this work, all these parameters were kept constant, only changing the pH of the solution (4, 6, 9.5, and 11). The production of ZnO NPs and their morphological dimensions were investigated using SEM images (Figure 3). Figure 3a,c,e,g demonstrates the effect of changing the pH of the solution (4, 6, 9.5, and 11) on the particle size and size distribution of the ZnO NPs.

The majority of the ZnO NPs were spherical or oval in form. ZnO NPs were aggregated, with a small number of dispersed single particles. The average size distribution of biosynthesized ZnO NPs is primarily about 70 nm, according to the particle size distribution histograms shown in Figure 3b,d,f, h. By comparing the size of the collected particles to the size of crystals, we can deduce that the particles are crystals.

ZnO NPs agglomeration is a process that reduces free surface energy by increasing particle size and decreasing surface area. The adherence of NPs to each other by weak forces causes agglomeration, which results in (sub) nanoentities [42].
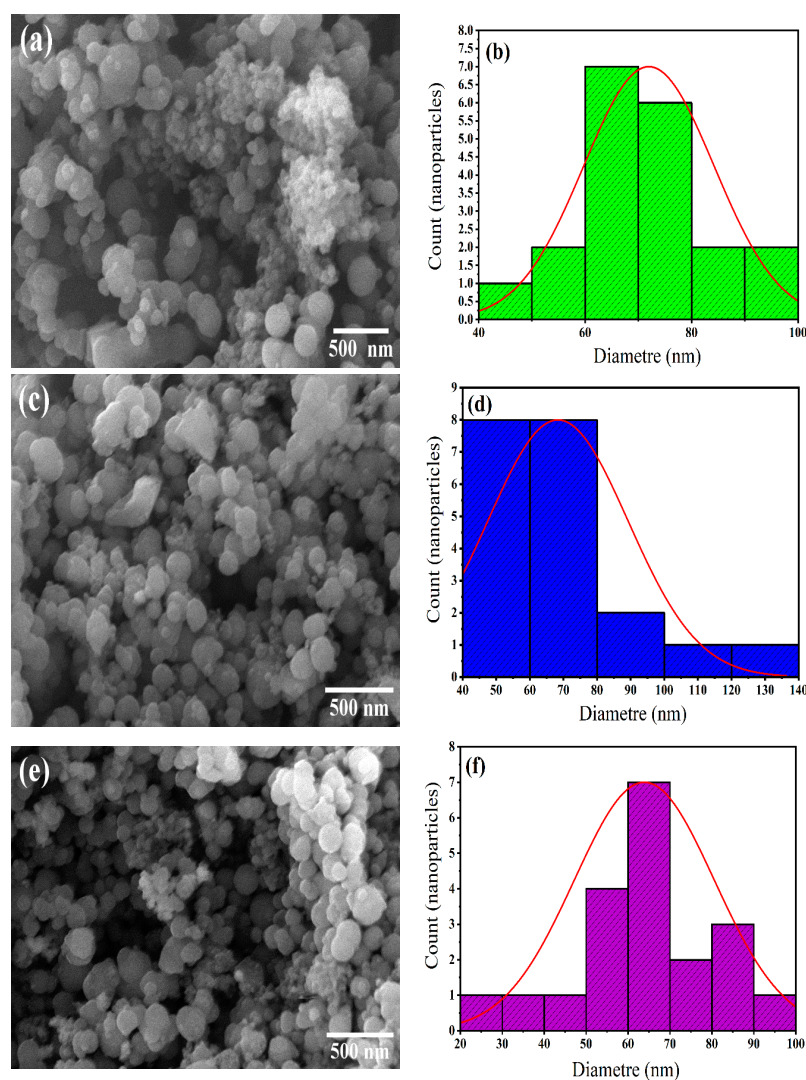

Figure 3. *Cont.*
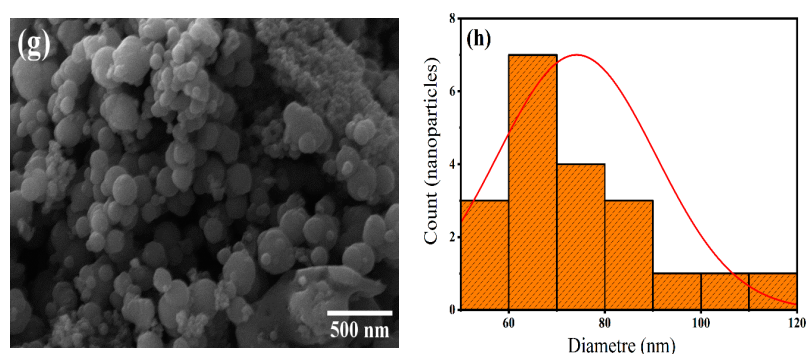
Figure 3. SEM images and particle size distributions of biosynthesis Zinc Oxide NPs with different pH values: (**a**,**b**) pH = 11, (**c**,**d**) pH = 9.5, (**e**,**f**) pH = 6, (**g**,**h**) pH = 4.

Further EDS examination of ZnO NPs verifies the existence of zinc and oxygen, as shown in Figure 4 and its related data, with a weight percentage of around 80.8% Zn and 18.56% O.
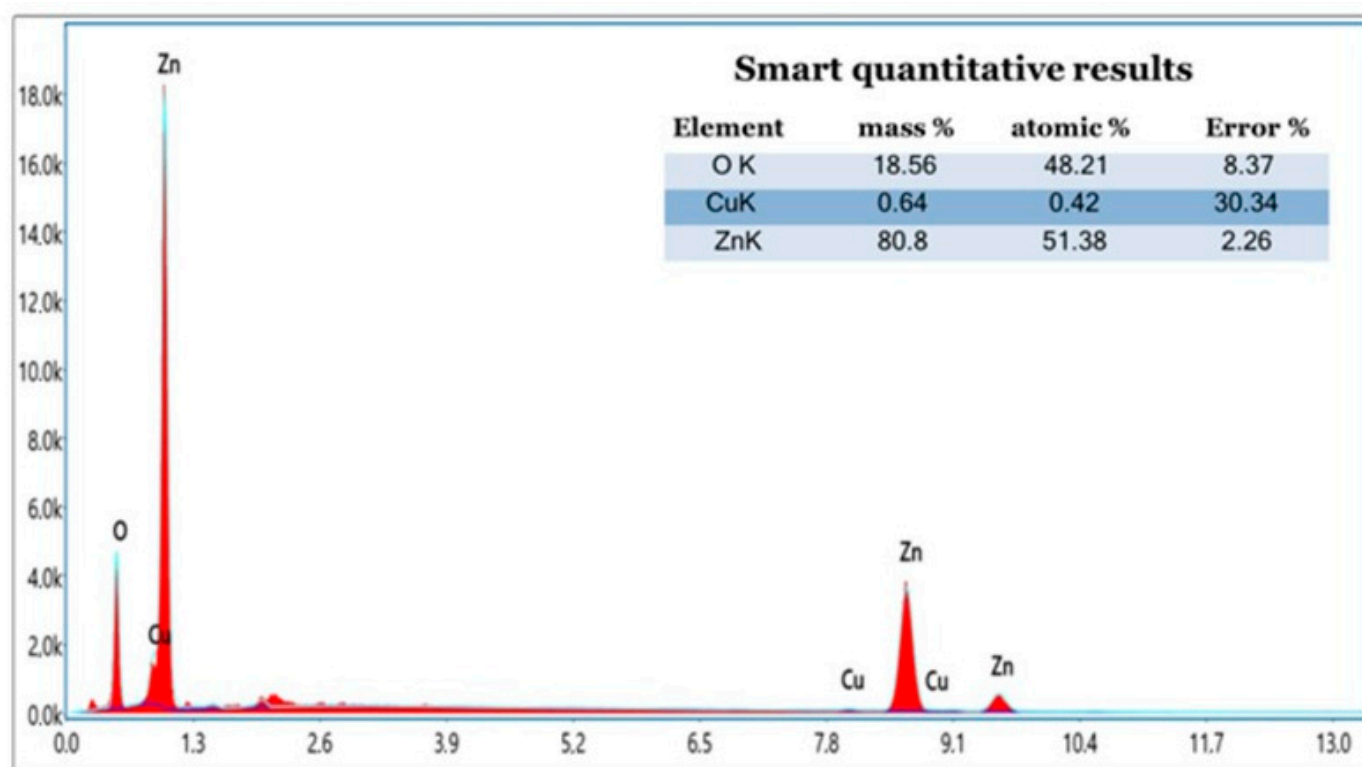

Smart quantitative results

Element	mass %	atomic %	Error %
O K	18.56	48.21	8.37
CuK	0.64	0.42	30.34
ZnK	80.8	51.38	2.26

Figure 4. EDS of Zinc Oxide Nanoparticles.

3.4. Bandgap and Optical characteristics

UV-Vis spectroscopy was used to evaluate the impact of different pH values (4, 6, 9.5, and 11) on the bio-reducing and capping agent of ZnO NPs.

The absorption spectra of the produced ZnO NPs at various pH values (4, 6, 9.5, and 11) are shown in Figure 5a. All assays were carried out with 3 g $Zn(CH_3COO)_2$. $2H_2O$ and fixing the concentration of plant extract, the temperature at 70 °C, and the concentration of Zn precursor.

A longer wavelength with a broad peak usually implies a larger particle size, whereas a shorter wavelength at a tight line usually results in smaller particle size [43].

The absorption spectra of NPs at varied pH values (4, 6, 9.5, and 11), fixed temperatures, and concentrations of plant extract and Zn precursor revealed the optical property of

generated ZnO NPs. These results perfectly agree with the literature, which claims that ZnO NPs exhibit characteristic surface plasmon peaks in the 350–380 nm wavelength range. The recording of the UV-Vis spectrum at pH = 6, and pH = 11, displayed a maximum absorbance peak at 378 nm, whereas, at pH = 4, a peak was observed at 350 nm, and at pH = 9.5, a comparatively narrow peak was recorded at 378 nm. Besides, the sharpness of the peak was increased with increasing pH.

The Tauc method is based on energy-dependent absorption coefficient α and which may be represented by the formula below Equation (4):

$$(\alpha h v) = A \left(h v - E_g^{opt} \right)^n \tag{4}$$

where h is the Planck constant, v is the frequency of the photon, E_g^{opt} is the energy of the band gap, and A is a constant. The n factor is equal to 1/2 or 2 for direct and indirect transition band gaps, respectively, depending on the type of the electron transition, as illustrated in Figure 5b,c. The optical bandgap energy for direct E_{g1}^{opt} and indirect E_{g2}^{opt} transitions can be estimated by plotting, and $(\alpha h v)^{1/2}$ vs photon energy (hv) [44]. The value of E_g^{opt} is obtained by extrapolating to $(h v \alpha)^2 = 0$ for direct transition and $(\alpha h v)^{1/2} = 0$ for indirect transition. As illustrated in Figure 5b,c and Table 2,

The direct bandgap increases from 2.97 to 3.97 eV, while the indirect bandgap increases from 2.15 to 2.74 eV when the pH rises from 4 to 11. According to previous research [45], direct and indirect energy gap estimations for synthesized ZnO NPs samples' semiconductor bandgap is 0–3 eV. These findings match a previous study that found the bandgap widens when particle size decreases [46]. The total concentration of ions, specifically H^+ and OH^-, directly affects the band gap of materials. The counter ions of the fist solvation shell will have an intimate relationship with electrons in a charged conducting material. The change in electron density generated by an ion's approximation will influence the material's band gap.

UV-vis spectra may detect the band tail energy, also known as Urbach energy E_u Equation (5). In the case of ZnO NPs formations, it has been discovered that as the crystal size increases, the Urbach energy values fall, resulting in decreasing crystallinity and structural disorder. The Urbach energy E_u is calculated using the reciprocal values of the slopes of the linear component of the $\ln(a)$ vs. photon energy hv (Figure 5d). Near the band edge, the absorption coefficient has an exponential relationship with photon energy (Urbach 1953) [47]. The computed Urbach energy values for the samples are shown in Table 2.

$$\ln a = \frac{hv}{E_u} + \text{ constant } (\ln a_0) \tag{5}$$

The Urbach energy E_u was calculated using the reciprocal of the slope of the linear fit section of the curve's photon energy. The latter is determined by the difference in energy between the ends of the tails of the valence and conduction bands: the lower the energy, the less turbulence. However, the disorder might alter depending on the presence of modifying oxides.

The Urbach energy Eu of the produced ZnO NPs decreases somewhat from 0.137 to 0.395 eV when the pH values are changed from 4 to 11, as shown in Table 2. Urbach energy findings have been attributed to structural and thermal instabilities. Such a variance in the band tail characteristic highlights the relevance of solution concentration as a defect source within the ZnO lattice [48].
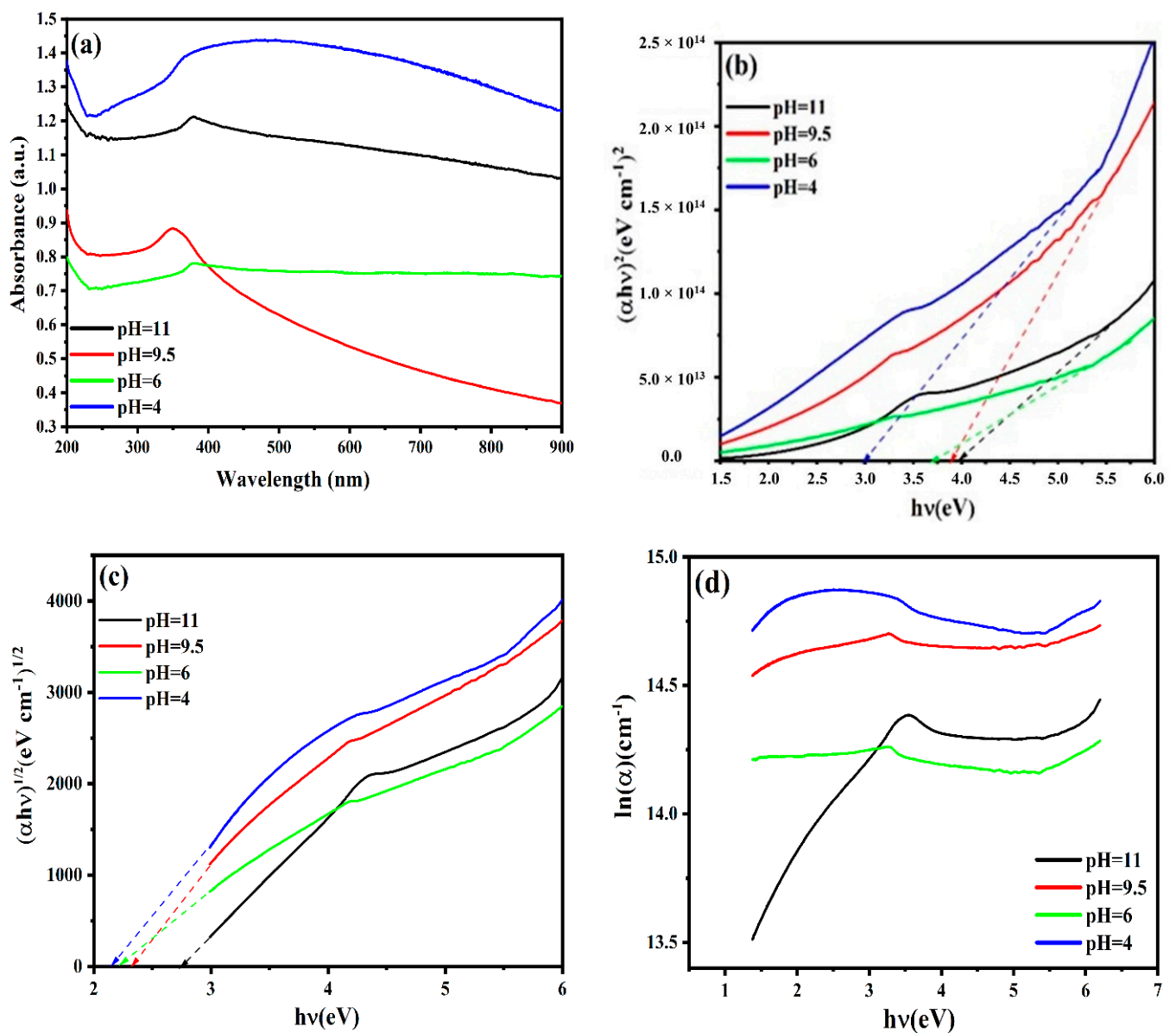
Figure 5. Optical properties of the ZnO NPs: UV-vis spectra (**a**); optical bandgap energy (**b**); indirect bandgap energy (**c**) transitions relying on Tauc's method; (**d**) Urbach energy.

Table 2. The effect of different pH values of ZnO NPs prepared using *Portulaca oleracea* L. extract and different pH values.

Samples	Direct OpticalBandgap (eV)	Indirect OpticalBandgap (eV)	Urbach Energy (eV)
pH = 11	3.97	2.74	0.137
pH = 9.5	3.90	2.32	0.154
pH = 6	3.69	2.21	0.215
pH = 4	2.97	2.15	0.395

3.5. Photocatalytic Activity of Zinc Oxide NPs for Azo Dye Degradation

Under solar irradiation, the photocatalytic degradation of MO was investigated using ZnO NPs at varied pH values (4, 6, 9.5, and 11), and the findings indicated that most of the

MO dye was decomposed after 120 min (Figure 6b,d,f,h). Where the different samples of ZnO NPs showed results very close.

ZnO NPs at pH 4 may be attributed to the small band gap (2.97 eV), compared with the ZnO NPs at pH = 6 (3.69 eV), pH = 9.5 (3.90 eV), and pH = 11 (3.97 eV), as a result of the shape of the NPs, which enhances photocatalytic degradation of organic dyes, as the geometrical shape plays an essential role in the reactivity of the NPs [49,50].

The environmental use of biosynthesized ZnO NPs was investigated using the aqueous solution of MO dye, and the findings are shown in Figure 6 a,c,e,g. According to the results, the first part of the experiment was conducted in the dark for 30 min to study the removal of pollutants via the adsorption pathway. The removal efficiencies due to adsorption were 31.70%, 29,75%, 31.42%, and 30.06% for the MO at the pH = 4, 6, 9.5 and 11, respectively. The photocatalytic properties of ZnO NPs on the degradation of MO dye—and it was discovered that the degradation occurred in two stages. The photodegradation process started quickly and then slowed down. The delayed deterioration in the second stage might be due to the difficulties of oxidizing the dye's N-atoms and the accumulated intermediates in the first stage, which slowed the oxidative photocatalytic reaction rate [51].

Below are the processes usually involved in the photocatalytic degradation of MO dye by ZnO NPs. The reactive species formed during irradiation of the ZnO NPs were h^+ (VB), OH·, and O^-_2, as stated by Equations (6)–(12), photoexcitation, charge separation and migration, and eventually surface oxidation-reduction processes, respectively [52].
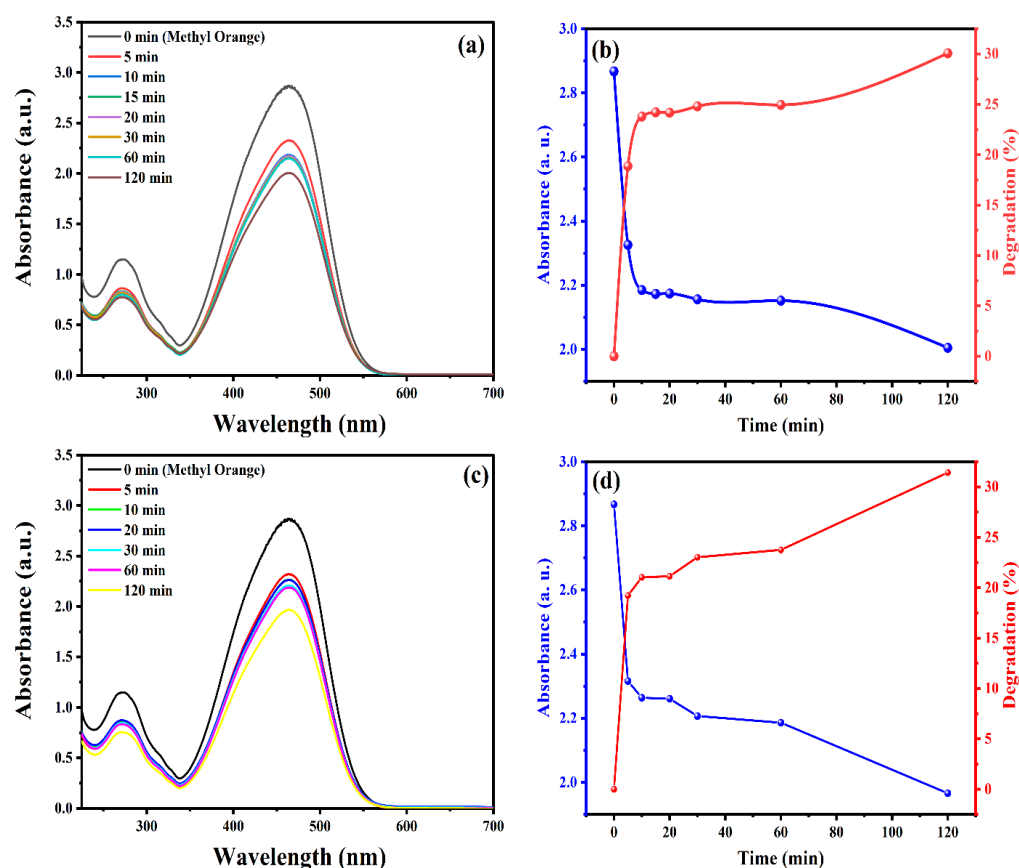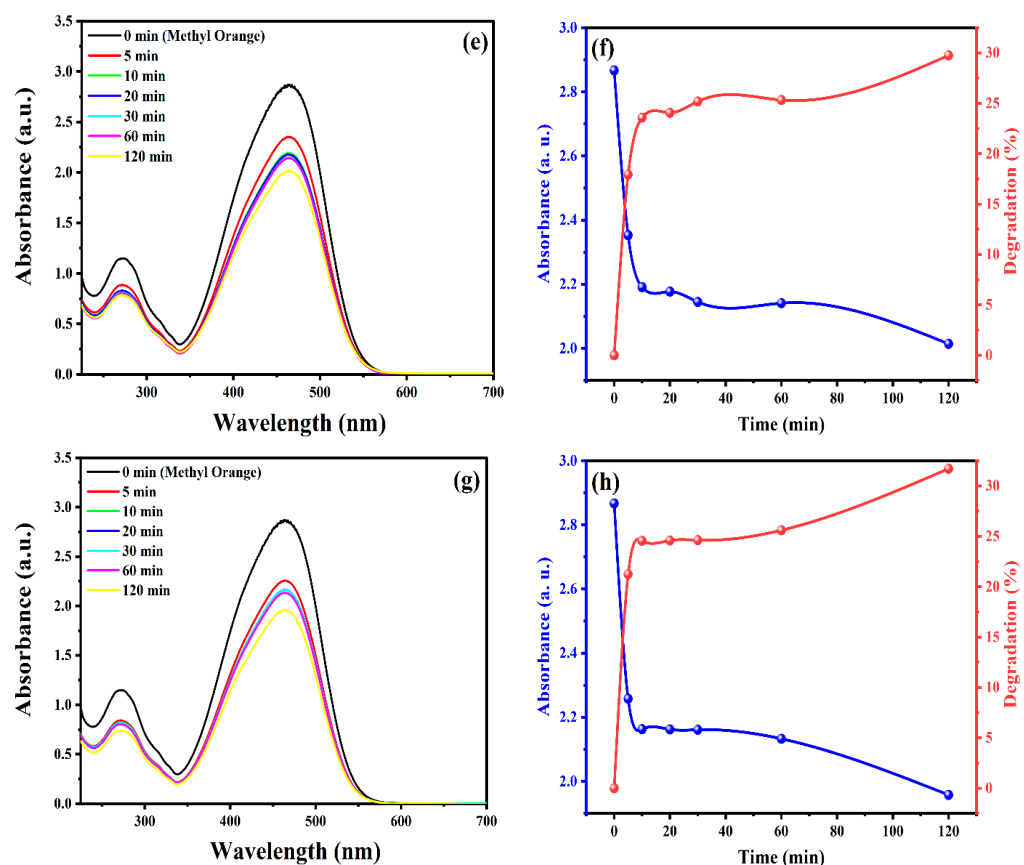

Figure 6. *Cont.*
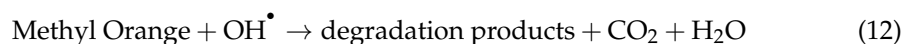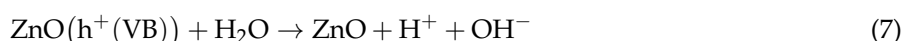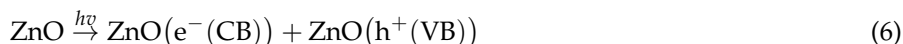
Figure 6. Time effect reaction of zinc oxide NPs on photodegradation of MO at different pH valuer (4, 6, 9.5, 11): (**a,b**) obtained by pH = 11, (**c,d**) obtained by pH = 9.5, (**e,f**) obtained by pH = 6, (**g,h**) obtained by pH = 4.

$$ZnO \xrightarrow{h\upsilon} ZnO\big(e^-(CB)\big) + ZnO\big(h^+(VB)\big) \tag{6}$$

$$ZnO\big(h^+(VB)\big) + H_2O \rightarrow ZnO + H^+ + OH^- \tag{7}$$

$$ZnO\big(e^-(CB)\big) + O_2 \rightarrow ZnO + O_2^{-\bullet} \tag{8}$$

$$H^+ + O_2^{-\bullet} \rightarrow HO_2^{\bullet} \tag{9}$$

$$HO_2^{\bullet} + HO_2^{\bullet} \rightarrow H_2O_2 + O_2 \tag{10}$$

$$H_2O_2 \xrightarrow{h\upsilon} 2OH^{\bullet} \tag{11}$$

$$\text{Methyl Orange} + OH^{\bullet} \rightarrow \text{degradation products} + CO_2 + H_2O \tag{12}$$

The suggested process for photocatalytic degradation of MO dye by ZnO NPs under sun irradiation is shown in Equations (6)–(12). Under solar irradiation of the ZnO NPs (Figure 7), electrons in the VB transfer to the CB, and the resulting energy is higher than the band gap of ZnO (2.97–3.97 eV), promoting the generation of valance band holes (h⁺) and conduction band electrons (e⁻), and possibly, the photogenerated holes at the VB coul could either directly oxidize the adsorbed MO dye or directly react with hydroxyl ((OH·). Meanwhile, photoelectrons at the CB might convert oxygen (O₂) adsorbed on the surface of ZnO NPs to superoxide radicals (O₂⁻·). As a result, both the produced OH and O₂⁻ may photocatalytically break down the MO dye [53–55].
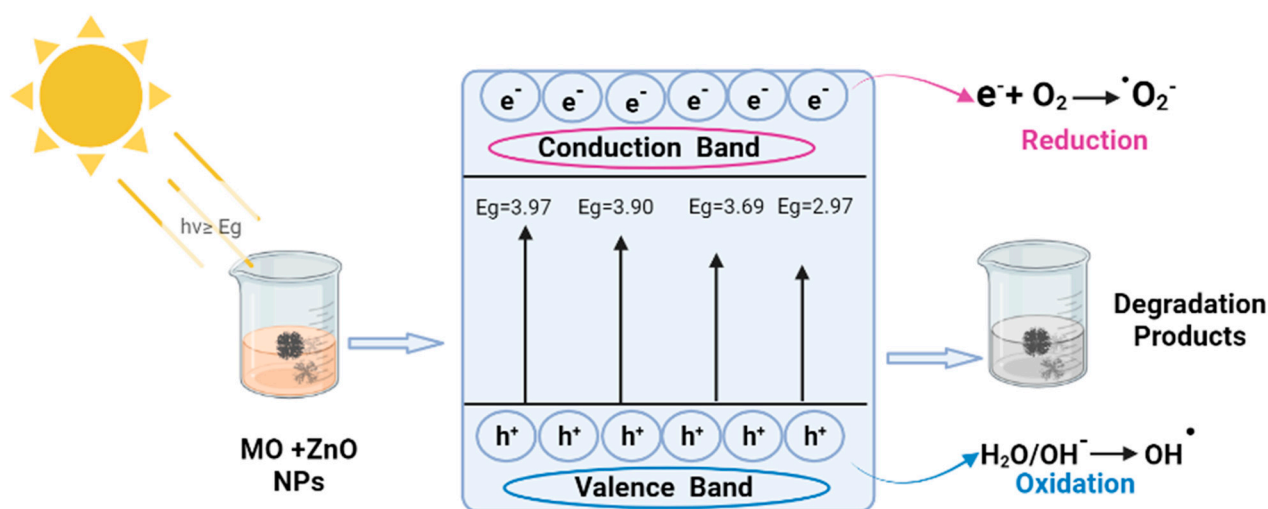
Figure 7. The mechanism by which Zinc Oxide nanoparticles are utilized for rapid photocatalytic degradation of methyl orange dye.

4. Conclusions

This study found that employing *Portulaca oleracea* leaf extract to synthesize ZnO NPs results in particles with different physical properties that substantially influence sorption attributes. The procedure is simple, quick, inexpensive, and ecologically benign, as it does not involve using organic solvents or other harmful chemicals. As a result, this synthesis process is more advantageous than traditional approaches for producing ZnO NPs. The produced ZnO NPs have a spherical, crystal-like form in nature. The crystallite diameters of ZnO NPs were calculated to be 22.17, 25.39, 22.98, and 27.38 nm, respectively, at pH = 11, pH = 9.5, pH = 6, and pH = 4. Furthermore, under environmental circumstances, the produced ZnO NPs exhibit high photocatalytic activity for dye degradation of methyl orange stains. In medicine, the substance ZnO NPs has been shown to be effective in treating wastewater (dye degradation).

Author Contributions: Conceptualization, B.G., S.E.L., S.M., A.B. (Abderrhmane Bouafia), F.M. and H.H.; methodology, B.G., A.B. (Abderrhmane Bouafia), S.M., G.T., F.M. and M.L.T.; validation, B.G., A.B. (Abderrhmane Bouafia), S.E.L., S.M., G.T., F.M. and M.L.T.; investigation, A.B. (Abderrhmane Bouafia), M.L.T., F.M. and S.M.; resources, B.G., A.B. (Ahmed Barhoum), and F.M.; data curation, B.G., A.B. (Abderrhmane Bouafia), M.L.T., G.T., F.M..; writing—original draft preparation, S.E.L., S.M., A.B. (Ahmed Barhoum), H.H, M.L.T., F.M.; writing—review and editing, A.B. (Ahmed Barhoum), S.M., M.L.T., G.T., F.M. and H.H.; supervision, A.B. (Ahmed Barhoum), S.E.L., S.M., F.M. and H.H. All authors have read and agreed to the published version of the manuscript.

Institutional Review Board Statement: Not applicable.

Informed Consent Statement: Not applicable.

Data Availability Statement: Not Applicable.

Conflicts of Interest: The authors declare no conflict of interest, financial or otherwise.

References

1. Faisal, S.; Jan, H.; Shah, S.A.; Shah, S.; Khan, A.; Akbar, M.T.; Rizwan, M.; Jan, F.; Wajidullah; Akhtar, N.; et al. Green Synthesis of Zinc Oxide (ZnO) Nanoparticles Using Aqueous Fruit Extracts of Myristica fragrans: Their Characterizations and Biological and Environmental Applications. *ACS Omega* **2021**, *6*, 9709–9722. [CrossRef] [PubMed]
2. Segets, D.; Gradl, J.; Taylor, R.K.; Vassilev, V.; Peukert, W. Analysis of Optical Absorbance Spectra for the Determination of ZnO Nanoparticle Size Distribution, Solubility, and Surface Energy. *ACS Nano* **2009**, *3*, 1703–1710. [CrossRef] [PubMed]
3. Rao, C.N.R.; Govindaraj, A. *Nanotubes and Nanowires*; RSC Nanoscience & Nanotechnology Series; RSC: London, UK, 2005.

4.   Wang, Z.L. Nanostructures of zinc oxide. *Mater. Today* **2004**, *7*, 26–33. [CrossRef]
5.   Zaouk, D.; Zaatar, Y.; Asmar, R.; Jabbour, J. Piezoelectric zinc oxide by electrostatic spray pyrolysis. *Microelectron. J.* **2006**, *37*, 1276–1279. [CrossRef]
6.   Ko, S.C.; Kim, Y.C.; Lee, S.S.; Choi, S.H.; Kim, S.R. Micromachined piezoelectric membrane acoustic device. *Sens. Actuators A Phys.* **2003**, *103*, 130–134. [CrossRef]
7.   Wijesinghe, U.; Thiripuranathar, G.; Iqbal, H.; Menaa, F. Biomimetic Synthesis, Characterization, and Evaluation of Fluorescence Resonance Energy Transfer, Photoluminescence, and Photocatalytic Activity of Zinc Oxide Nanoparticles. *Sustainability* **2021**, *13*, 2004. [CrossRef]
8.   Wijesinghe, U.; Thiripuranathar, G.; Menaa, F.; Almukhlifi, H. Eco-friendly Synthesis of Zinc Oxide Nanoparticles and Assessment of its Activities as Efficient Antioxidant Agent. *Curr. Nanosci.* **2022**, *18*, 1. [CrossRef]
9.   Daniel, M. *Medicinal Plants: Chemistry and Properties*; Science Publishers: New York, NY, USA, 2006; ISBN 1578083958.
10. Cui, M.Z.; Liu, H.; Li, C.Y. Changes of blood glucose in diabetic rats and the interventional effect of purslane. *Chin. J. Clin. Rehabil.* **2005**, *27*, 92–93.
11. El-Sayed, M.-I.K. Effects of *Portulaca oleracea* L. seeds in treatment of type-2 diabetes mellitus patients as adjunctive and alternative therapy. *J. Ethnopharmacol.* **2011**, *137*, 643–651. [CrossRef]
12. Movahedian, A.; Ghannadi, A.; Vashirnia, M. Hypocholesterolemic effects of purslane extract on serum lipids in rabbits fed with high cholesterol levels. *Int. J. Pharmacol.* **2007**, *3*, 285–289.
13. Li, Y.-H.; Lai, C.-Y.; Su, M.-C.; Cheng, J.-C.; Chang, Y.-S. Antiviral activity of *Portulaca oleracea* L. against influenza A viruses. *J. Ethnopharmacol.* **2019**, *241*, 112013. [CrossRef] [PubMed]
14. Lim, Y.Y.; Quah, E.P.L. Antioxidant properties of different cultivars of *Portulaca oleracea*. *Food Chem.* **2007**, *103*, 734–740. [CrossRef]
15. Gunenc, A.; Rowland, O.; Xu, H.; Marangoni, A.; Hosseinian, F. *Portulaca oleracea* seeds as a novel source of alkylresorcinols and its phenolic profiles during germination. *LWT* **2019**, *101*, 246–250. [CrossRef]
16. Culpeper, N. *Culpeper's Complete Herbal: A Book of Natural Remedies for Ancient Ills*; Wordsworth Editions: Hertfordshire, UK, 1995; ISBN 1853263451.
17. Zyoud, A.H.; Zubi, A.; Zyoud, S.H.; Hilal, M.H.; Zyoud, S.; Qamhieh, N.; Hajamohideen, A.; Hilal, H.S. Kaolin-supported ZnO nanoparticle catalysts in self-sensitized tetracycline photodegradation: Zero-point charge and pH effects. *Appl. Clay Sci.* **2019**, *182*, 105294. [CrossRef]
18. Shetti, N.P.; Malode, S.J.; Nayak, D.S.; Bagihalli, G.B.; Kalanur, S.S.; Malladi, R.S.; Reddy, C.V.; Aminabhavi, T.M.; Reddy, K.R. Fabrication of ZnO nanoparticles modified sensor for electrochemical oxidation of methdilazine. *Appl. Surf. Sci.* **2019**, *496*, 143656. [CrossRef]
19. Arya, S.; Mahajan, P.; Mahajan, S.; Khosla, A.; Datt, R.; Gupta, V.; Young, S.-J.; Oruganti, S.K. Review—Influence of Processing Parameters to Control Morphology and Optical Properties of Sol-Gel Synthesized ZnO Nanoparticles. *ECS J. Solid State Sci. Technol.* **2021**, *10*, 23002. [CrossRef]
20. Khairol, N.F.; Sapawe, N. Electrosynthesis of ZnO nanoparticles deposited onto egg shell for degradation of Congo red. *Mater. Today Proc.* **2018**, *5*, 21936–21939. [CrossRef]
21. Bouafia, A.; Laouini, S.E.; Khelef, A.; Tedjani, M.L.; Guemari, F. Effect of Ferric Chloride Concentration on the Type of Magnetite (Fe$_3$O$_4$) Nanoparticles Biosynthesized by Aqueous Leaves Extract of Artemisia and Assessment of Their Antioxidant Activities. *J. Clust. Sci.* **2021**, *32*, 1033–1041. [CrossRef]
22. Laouini, S.E.; Bouafia, A.; Soldatov, A.V.; Algarni, H.; Tedjani, M.L.; Ali, G.A.M.; Barhoum, A. Green Synthesized of Ag/Ag$_2$O Nanoparticles Using Aqueous Leaves Extracts of *Phoenix dactylifera* L. and Their Azo Dye Photodegradation. *Membranes* **2021**, *11*, 468. [CrossRef]
23. Bouafia, A.; Laouini, S.E. Green synthesis of iron oxide nanoparticles by aqueous leaves extract of *Mentha Pulegium* L.: Effect of ferric chloride concentration on the type of product. *Mater. Lett.* **2020**, *265*, 127364. [CrossRef]
24. Daoudi, H.; Bouafia, A.; Meneceur, S.; Laouini, S.E.; Belkhalfa, H.; Lebbihi, R.; Selmi, B. Secondary Metabolite from Nigella Sativa Seeds Mediated Synthesis of Silver Oxide Nanoparticles for Efficient Antioxidant and Antibacterial Activity. *J. Inorg. Organomet. Polym. Mater.* **2022**. [CrossRef]
25. Bouafia, A.; Laouini, S.E.; Ahmed, A.S.A.; Soldatov, A.V.; Algarni, H.; Feng Chong, K.; Ali, G.A.M. The Recent Progress on Silver Nanoparticles: Synthesis and Electronic Applications. *Nanomaterials* **2021**, *11*, 2318. [CrossRef] [PubMed]
26. Bouafia, A.; Laouini, S.E. Plant-Mediated Synthesis of Iron Oxide Nanoparticles and Evaluation of the Antimicrobial Activity: A Review. *Mini. Rev. Org. Chem.* **2020**, *18*, 725–734. [CrossRef]
27. Rashed, M.N.; El-Amin, A. Photocatalytic degradation of methyl orange in aqueous TiO$_2$ under different solar irradiation sources. *Int. J. Phys. Sci.* **2007**, *2*, 73–81.
28. Wang, G.-S.; Liao, C.-H.; Wu, F.-J. Photodegradation of humic acids in the presence of hydrogen peroxide. *Chemosphere* **2001**, *42*, 379–387. [CrossRef]
29. Khan, A.B.; Kathi, S. Evaluation of heavy metal and total petroleum hydrocarbon contamination of roadside surface soil. *Int. J. Environ. Sci. Technol.* **2014**, *11*, 2259–2270. [CrossRef]
30. Uzair, B.; Liaqat, A.; Iqbal, H.; Menaa, B.; Razzaq, A.; Thiripuranathar, G.; Fatima Rana, N.; Menaa, F. Green and Cost-Effective Synthesis of Metallic Nanoparticles by Algae: Safe Methods for Translational Medicine. *Bioengineering* **2020**, *7*, 129. [CrossRef]

31. Al-Otibi, F.; Alfuzan, S.A.; Alharbi, R.I.; Al-Askar, A.A.; AL-Otaibi, R.M.; Al Subaie, H.F.; Moubayed, N.M.S. Comparative study of antifungal activity of two preparations of green silver nanoparticles from *Portulaca oleracea* extract. *Saudi J. Biol. Sci.* **2022**, *29*, 2772–2781. [CrossRef]

32. Lee, Y.J.; Park, Y. Graphene oxide grafted gold nanoparticles and silver/silver chloride nanoparticles green-synthesized by a *Portulaca oleracea* extract: Assessment of catalytic activity. *Colloids Surfaces A Physicochem. Eng. Asp.* **2020**, *607*, 125527. [CrossRef]

33. Oves, M.; Aslam, M.; Rauf, M.A.; Qayyum, S.; Qari, H.A.; Khan, M.S.; Alam, M.Z.; Tabrez, S.; Pugazhendhi, A.; Ismail, I.M.I. Antimicrobial and anticancer activities of silver nanoparticles synthesized from the root hair extract of Phoenix dactylifera. *Mater. Sci. Eng. C* **2018**, *89*, 429–443. [CrossRef]

34. Simopoulos, A.P.; Norman, H.A.; Gillaspy, J.E.; Duke, J.A. Common purslane: A source of omega-3 fatty acids and antioxidants. *J. Am. Coll. Nutr.* **1992**, *11*, 374–382. [CrossRef] [PubMed]

35. Kihara, K.; Donnay, G. Anharmonic thermal vibrations in ZnO. *Can. Mineral.* **1985**, *23*, 647–654.

36. El-Desouky, T.A. Evaluation of effectiveness aqueous extract for some leaves of wild edible plants in Egypt as anti-fungal and anti-toxigenic. *Heliyon* **2021**, *7*, e06209. [CrossRef]

37. Patil, R.B.; Chougale, A.D. Analytical methods for the identification and characterization of silver nanoparticles: A brief review. *Mater. Today Proc.* **2021**, *47*, 5520–5532. [CrossRef]

38. Raj, A.; Lawrence, R.; Lawrence, K.; Silas, N.; Jaless, M.; Srivastava, R. Green synthesis and charcterization of silver nanoparticles from leafs extracts of rosa indica and its antibacterial activity against human pathogen bacteria. *Orient. J. Chem.* **2018**, *34*, 326–335. [CrossRef]

39. Xu, X.; Yu, L.; Chen, G. Determination of flavonoids in *Portulaca oleracea* L. by capillary electrophoresis with electrochemical detection. *J. Pharm. Biomed. Anal.* **2006**, *41*, 493–499. [CrossRef]

40. Handore, K.; Bhavsar, S.; Horne, A.; Chhattise, P.; Mohite, K.; Ambekar, J.; Pande, N.; Chabukswar, V. Novel Green Route of Synthesis of ZnO Nanoparticles by Using Natural Biodegradable Polymer and Its Application as a Catalyst for Oxidation of Aldehydes. *J. Macromol. Sci. Part A* **2014**, *51*, 941–947. [CrossRef]

41. Hoseinpour, V.; Souri, M.; Ghaemi, N.; Shakeri, A. Optimization of green synthesis of ZnO nanoparticles by *Dittrichia graveolens* (L). *aqueous extract.* **2017**, *1*, 39–49. [CrossRef]

42. Gosens, I.; Post, J.A.; de la Fonteyne, L.J.; Jansen, E.H.; Geus, J.W.; Cassee, F.R.; de Jong, W.H. Impact of agglomeration state of nano-and submicron sized gold particles on pulmonary inflammation. *Part. Fibre Toxicol.* **2010**, *7*, 37. [CrossRef]

43. Khan, M.; Khan, M.; Adil, S.F.; Tahir, M.N.; Tremel, W.; Alkhathlan, H.Z.; Al-Warthan, A.; Siddiqui, M.R.H. Green synthesis of silver nanoparticles mediated by Pulicaria glutinosa extract. *Int. J. Nanomedicine* **2013**, *8*, 1507–1516. [CrossRef]

44. Bouafia, A.; Laouini, S.E.; Tedjani, M.L.; Ali, G.A.M.; Barhoum, A. Green biosynthesis and physicochemical characterization of Fe$_3$O$_4$ nanoparticles using *Punica granatum* L. fruit peel extract for optoelectronic applications. *Text. Res. J.* **2022**, *92*, 2685–2696. [CrossRef]

45. Fuku, X.; Modibedi, M.; Mathe, M. Green synthesis of Cu/Cu$_2$O/CuO nanostructures and the analysis of their electrochemical properties. *SN Appl. Sci.* **2020**, *2*, 902. [CrossRef]

46. Kulkarni, S.A.; Sawadh, P.S.; Palei, P.K.; Kokate, K.K. Effect of synthesis route on the structural, optical and magnetic properties of Fe$_3$O$_4$ nanoparticles. *Ceram. Int.* **2014**, *40*, 1945–1949. [CrossRef]

47. Urbach, F. The Long-Wavelength Edge of Photographic Sensitivity and of the Electronic Absorption of Solids. *Phys. Rev.* **1953**, *92*, 1324. [CrossRef]

48. Vasile, O.-R.; Andronescu, E.; Ghitulica, C.; Vasile, B.S.; Oprea, O.; Vasile, E.; Trusca, R. Synthesis and characterization of nanostructured zinc oxide particles synthesized by the pyrosol method. *J. Nanoparticle Res.* **2012**, *14*, 1269. [CrossRef]

49. Basnet, P.; Inakhunbi Chanu, T.; Samanta, D.; Chatterjee, S. A review on bio-synthesized zinc oxide nanoparticles using plant extracts as reductants and stabilizing agents. *J. Photochem. Photobiol. B Biol.* **2018**, *183*, 201–221. [CrossRef]

50. Balázs, N.; Mogyorósi, K.; Srankó, D.F.; Pallagi, A.; Alapi, T.; Oszkó, A.; Dombi, A.; Sipos, P. The effect of particle shape on the activity of nanocrystalline TiO$_2$ photocatalysts in phenol decomposition. *Appl. Catal. B Environ.* **2008**, *84*, 356–362. [CrossRef]

51. Blaskov, V.N.; Stambolova, I.D.; Milenova, K.I.; Zaharieva, K.L.; Dimitrov, L.D.; Stoyanova, D.D.; Eliyas, A.E. The photodegradation of Methylene Blue and Methyl Orange dyes and their mixture by ZnO obtained by hydrothermally activated precipitates. *Bulg. Chem. Commun* **2017**, *49*, 183–187.

52. Li, H.; Yin, S.; Wang, Y.; Sato, T. Efficient persistent photocatalytic decomposition of nitrogen monoxide over a fluorescence-assisted CaAl$_2$O$_4$:(Eu, Nd)/(Ta, N)-codoped TiO$_2$/Fe$_2$O$_3$. *Appl. Catal. B Environ.* **2013**, *132–133*, 487–492. [CrossRef]

53. Palanisamy, B.; Babu, C.M.; Sundaravel, B.; Anandan, S.; Murugesan, V. Sol–gel synthesis of mesoporous mixed Fe$_2$O$_3$/TiO$_2$ photocatalyst: Application for degradation of 4-chlorophenol. *J. Hazard. Mater.* **2013**, *252–253*, 233–242. [CrossRef] [PubMed]

54. Chen, X.; Wu, Z.; Liu, D.; Gao, Z. Preparation of ZnO Photocatalyst for the Efficient and Rapid Photocatalytic Degradation of Azo Dyes. *Nanoscale Res. Lett.* **2017**, *12*, 143. [CrossRef] [PubMed]

55. Li, Z.; Liu, G.; Su, Q.; Lv, C.; Jin, X.; Wen, X. UV-Induced Photodegradation of Naproxen Using a Nano γ-FeOOH Composite: Degradation Kinetics and Photocatalytic Mechanism. *Front. Chem.* **2019**, *7*, 847. [CrossRef] [PubMed]